Nonequilibrium molecular dynamics study of shear and shearfree flows in simple fluids

András Baranyai and Peter T. Cummings

Citation: The Journal of Chemical Physics **103**, 10217 (1995); doi: 10.1063/1.469925
View online: http://dx.doi.org/10.1063/1.469925
View Table of Contents: http://scitation.aip.org/content/aip/journal/jcp/103/23?ver=pdfcov
Published by the AIP Publishing

Nonequilibrium molecular dynamics study of shear and shear-free flows in simple fluids

András Baranyai[a] and Peter T. Cummings
Department of Chemical Engineering, University of Tennessee, Knoxville, Tennessee 37996-2200
and Chemical Technology Division, Oak Ridge National Laboratory, Oak Ridge, Tennessee 37831-6268

(Received 3 January 1995; accepted 14 September 1995)

Nonequilibrium molecular dynamics simulations have been performed in order to compare the characteristics of planar Couette, planar elongation, uniaxial stretching, and biaxial stretching flows in simple fluids at different strain rates. After deriving the periodic boundary conditions for general flow fields and introducing some methodological improvements for elongation flow calculations we simulated the combination of shear and shear-free flows as well. We found that even at high strain rates where simple fluids exhibit strong non-Newtonian behavior (shear-thinning) it is a reasonable approximation to consider the two planar flows to be rotationally equivalent. This is because in planar Couette flow the in-plane normal stress difference of simple fluids is approximately zero even far from equilibrium. Similarly to planar Couette flow, the trace of the pressure tensor and the internal energy vary approximately as function of the 3/2 power of the strain rate in shear free flows. However, the individual diagonal elements of elongation flow pressure tensors deviate considerably from this approximation. In the extension direction the pressure seems to have a minimum in terms of the strain rate in every shear-free flow. We have discussed the implications of these results. © *1995 American Institute of Physics.*

I. INTRODUCTION

In the rheology of polymeric fluids, one invariably distinguishes between two classes of viscometric flows used to experimentally characterize a polymeric fluid—shear flows and shear-free flows—and these two classes of flows receive similar attention in texts devoted to the rheology of polymeric fluids.[1] By contrast, there are numerous computer simulations reported in the literature for shearing liquids studied at the atomic/molecular level but very few for shear free or elongation flows. This disparity is caused by implementation problems of elongation flow simulations. While in shearing liquids the boundary conditions make possible a long, steady state simulation of the system, in elongation flows the exponentially fast deformation of the system box sets a limit on the time range available for study. To our knowledge there are two previous sets of papers reporting about nonequilibrium molecular dynamics (NEMD) simulations of shear free flows. The first step in this direction was reported by Heyes.[2,3] More recently Ryckaert and coworkers published the results of systematic studies for atomistic[4] and molecular[5] liquids.

In this paper we report results of planar Couette flow (PCF), planar elongation flow (PEF), biaxial stretching flow (BSF), and uniaxial stretching flow (USF) calculations and also combinations of shear and shear-free flows. We begin by reviewing the relationship between shear and shear-free flows under conditions close to equilibrium. Although the following symmetry arguments are well-known to the researchers of fluid dynamics or rheology it might be useful to the reader to see the equilibrium behavior when interpreting the discrepancies between the different flows far from equilibrium.

The shear viscosity, η, of an equilibrium liquid is given by the Green–Kubo (GK) relations[6–8]

$$\eta=\frac{V}{kT}\int_0^\infty dt\langle P_{xy}(t)P_{xy}(0)\rangle, \tag{1}$$

where k is Boltzmann's constant, V is the volume, T is the temperature, and P_{xy} is the xy element of the pressure tensor, $\mathbf{P}$ of the system. (It should be noted here that P_{xy}, P_{xz}, and P_{yz} are fluctuating independently, so the average of these three autocorrelation functions can improve the statistics of viscosity calculations.) In addition to Eq. (1), there is another GK expression containing the shear viscosity,[6,7]

$$\eta_b+\frac{4}{3}\eta=\frac{V}{kT}\int_0^\infty dt\langle[(P_{xx}(t)-P][P_{xx}(0)-P]\rangle, \tag{2}$$

where η_b is the bulk viscosity and $P=1/3\ \mathrm{Tr}(\mathbf{P})$ is the average of the hydrostatic pressure. If we combine Eq. (2) with the more customary GK expression for bulk viscosity

$$\eta_b=\frac{V}{kT}\int_0^\infty dt\langle[(P(t)-P][P(0)-P]\rangle, \tag{3}$$

it becomes obvious that the shear viscosity can be expressed as a GK integral of combinations of diagonal elements of the pressure tensor. Indeed, the following integral also gives the shear viscosity

$$\eta=\frac{V}{kT}\int_0^\infty dt\frac{1}{m}\langle[\Delta P(t)][\Delta P(0)]\rangle, \tag{4}$$

where there are two different possible definitions of ΔP. If $\Delta P=P_{xx}-P_{yy}$ then $m=4$. The second possibility is when $\Delta P=P_{xx}-(P_{yy}+P_{zz})/2$ then $m=3$. These two GK integrals are identical if one takes the averages of all possible

[a]Permanent address: Eötvös University, Laboratory of Theoretical Chemistry, Budapest 112, P.O. Box 32, 1518-Hungary.

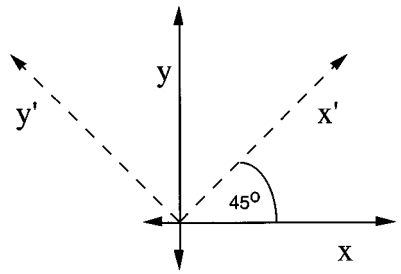

FIG. 1. The shear plane of PCF. Particles flow in the x direction with a constant velocity gradient in the y direction. The x' and y' axes give the corresponding extending and contracting directions, respectively, for the corresponding PEF.

combinations of directions. (This implies that if one wishes to reduce the statistical noise in the calculation of η, there is no point in calculating both types of these correlation functions. At every instant the pressure tensor has only six-independent elements and this gives the maximum number of functions we can utilize in numerical calculations.[9]) Equation (4) can also be derived directly assuming a shear free velocity gradient tensor,

$$\boldsymbol{\kappa}=\nabla\boldsymbol{\mu}=\begin{pmatrix}\dot{\epsilon}_x & 0 & 0\\ 0 & \dot{\epsilon}_y & 0\\ 0 & 0 & \dot{\epsilon}_z\end{pmatrix} \tag{5}$$

which gives for the strain rate tensor

$$\dot{\boldsymbol{\gamma}}=\boldsymbol{\kappa}+\boldsymbol{\kappa}^T=\begin{pmatrix}2\dot{\epsilon}_x & 0 & 0\\ 0 & 2\dot{\epsilon}_y & 0\\ 0 & 0 & 2\dot{\epsilon}_z\end{pmatrix}. \tag{6}$$

In this equation, $\dot{\epsilon}_\alpha$ is the dilation rate in the corresponding, α, direction. We consider only volume preserving flows in which the sum of the diagonal elements is zero. If one of the elements is zero then the flow field is referred to as planar elongation flow (PEF);[1] in uniaxial stretching flow (USF), one element is positive and the other two are equal but negative.[1] In the case of biaxial stretching flow (BSF) two elements are equal and positive.[1] If we define the viscosity following Ref. 5 as

$$\eta=(\boldsymbol{\sigma}\dot{\boldsymbol{\gamma}})/(\dot{\boldsymbol{\gamma}}:\dot{\boldsymbol{\gamma}}), \tag{7}$$

where $\boldsymbol{\sigma}$ is the stress tensor, the derivation of a Green–Kubo expression of the form given in Eq. (4) for these three type of flows is easily reproduced using, for example, the procedure given in Ref. 8. For PEF we obtain the first version of Eq. (4) while for USF and BSF we obtain the second one.

The validity of Eq. (4) is justified more simply just by referring to the existence of rotational or frame invariance in an equilibrium liquid. If we take the pressure tensor of an equilibrium liquid and define a new frame of reference which is tilted by 45° in the $x-y$ plane (see Fig. 1) then we obtain the following expression for the pressure tensor in the new frame:

$$\mathbf{P}=\frac{1}{2}\begin{pmatrix}P_{xx}+P_{yy}+2P_{xy} & P_{yy}-P_{xx} & 0\\ P_{yy}-P_{xx} & P_{xx}+P_{yy}-2P_{xy} & 0\\ 0 & 0 & 2P_{zz}\end{pmatrix}, \tag{8}$$

where, for the sake of simplicity, we put zeros in the off-diagonal elements containing z.

Now, we can see that at equilibrium, where the fluid is isotropic, the autocorrelation function of the xy element in the new frame corresponds to an autocorrelation function given by the difference of diagonal elements in the original frame and vice versa. Thus, at equilibrium, the response of a system to a PEF field is indistinguishable from the response to a PCF field. Here we adopt the convention that the planar shear flow takes place in the xy plane; particles moving with streaming velocity in the x direction while there is a uniform streaming velocity gradient along the y axis. Indeed, in the case of a liquid of symmetric top molecules we know that in the linear regime the average orientation of a molecule is 45° in the xy plane while it is rotating with an average speed of $\omega_z=-\dot{\gamma}/2$.[10,11] We cannot distinguish this motion from a PEF flow in the second frame where the average orientation of a molecule is parallel with the direction of extension.

It should be noted before proceeding further that the velocity field and the strain rate tensor of PCF should also be transformed into the new frame to obtain identical viscosities at small fields. From this transformation we learn that one needs twice as strong PEF velocity field to obtain the same response in the stress tensor.

II. ROTATIONAL CORRESPONDENCE OF PEF AND PCF FLOWS OUTSIDE THE LINEAR REGIME

The rotational equivalence of PCF and PEF in the linear regime is valid because there are no normal stress effects present in the diagonal elements. In fact, it is the in-plane stress difference, $P_{yy}-P_{xx}$, which should be negligible for this similarity to be hold. NEMD simulations of simple liquids characterized by short-range spherically symmetric intermolecular potentials (such as the Lennard-Jones potential) show that this property of the pressure tensor is maintained far outside the linear regime. While out-of-plane stress differences are increasing with shear rate in the same fashion as the off-diagonal stress, in-plane stress differences remain very small, most of the times within the error bars of pressure calculations.[8] Thus, we propose that for simple fluids the PCF and PEF flow fields are rotationally equivalent even in the nonlinear regime.

In Table I we show results of PCF calculations for a system of 500 WCA particles. This spherically symmetric, pairwise additive short-range interaction, $\phi(r)$, is defined in terms of the distance between two particles, r, as follows:

$$\phi(r)\begin{cases}4\left[\dfrac{1}{r^{12}}-\dfrac{1}{r^6}\right]+1, & r<2^{1/6}\\ 0, & r>2^{1/6}\end{cases}.$$

Here we used the usual reduced units of computer simulations [distances made dimensionless by dividing by the molecule diameter σ, energies made dimensionless by dividing

TABLE I. Values of pressure tensor elements of planar Couette flow simulations at different reduced shear rates ($T=0.722$, $\rho=0.8442$, $N=500$ WCA particles). Estimated error in the data ± 0.010.

$\dot{\gamma}$	P_{xx}	P_{yy}	P_{zz}	P_{xy}
0.00	6.406	6.406	6.406	0.000
0.25	6.498	6.513	6.473	−0.542
0.50	6.691	6.722	6.597	−1.000
0.75	6.941	6.986	6.751	−1.418
1.00	7.235	7.282	6.922	−1.807
1.25	7.574	7.617	7.130	−2.177
1.50	7.933	7.980	7.347	−2.524

by the characteristic interaction energy ϵ, temperature made dimensionless by multiplying by k/ϵ where k is Boltzmann's constant, number densities made dimensionless by multiplying by σ^3, strain rates made dimensionless by multiplying by $(m\sigma^2/\epsilon)^{1/2}$, and times made dimensionless by dividing by $(m\sigma^2/\epsilon)^{1/2}$].[7] The temperature, $T=0.722$, and the number density, $\rho=0.8442$, correspond to the triple point conditions of liquid argon. We used only the half of the usual timestep, $\Delta t=0.002$, in order to have higher accuracy. A fifth-order Gear algorithm integrated the equations of motion. The length of each run was 2 million timesteps, i.e., 4000 time units.

The proposed rotational equivalence of PEF and PCF flows for simple liquids in the nonlinear regime can be confirmed using the data of Pierloni and Ryckaert[4] who also studied a fluid of WCA particles but at a different state point. These authors plotted their PEF and PCF viscosities calculated from separate shear and shear free simulations on the same graph in terms of $\dot{\epsilon}, \dot{\gamma}$ using the definition of Eq. (7). At zero rate the two curves matched but for higher shear or elongational rates the PEF viscosities were systematically below the shear viscosities. They also made a plot of viscosities in terms of the second scalar invariants of the strain-rate tensor, II, which is $2\dot{\gamma}^2$ for PCF and $4\dot{\epsilon}^2$ for PEF, and they reported that the two types of viscosity data fell on the same curve within statistical errors.

This behavior can be explained in terms of the proposed rotational equivalence of these two flows. The viscosity of simple fluids in terms of the shear rate can be approximated as follows:

$$\eta(\dot{\gamma}) = \eta_0 - \eta_1\sqrt{\dot{\gamma}}. \tag{9}$$

For PEF field in the tilted coordinate frame this suggests that

$$\eta(\dot{\epsilon}) = \eta_0 - \eta_1\sqrt{2\dot{\epsilon}}. \tag{10}$$

Taking the two equations above into account it is clear that in terms of the second scalar invariants of the strain-rate tensor the viscosities will fall on the same curve if the proposed rotational equivalence is assumed.

The other two shear free flows (USF, BSF) cannot be as simply related to shear flow under these conditions. Both of the latter flows can be decomposed into two PEF fields acting in perpendicular planes. (In this way they can also be considered to be the superposition of two perpendicular shear fields.) Before pursuing the subject of more complicated homogeneous flow fields like combinations of shear and shear free flows, we devote some effort to the problem of periodic boundary conditions in NEMD simulations. We are motivated to do so because combined flow fields present subtleties which were apparently overlooked in previous work.[3]

III. METHODOLOGY FOR VISCOUS FLOW NEMD CALCULATIONS

A. Periodic boundary conditions for arbitrary flows

In the most general treatment of this problem one must follow the time evolution of a fluid element which in simulations is represented by a box containing the particles. We can arrange the elements of three noncoplanar vectors, $\mathbf{L}_1$, $\mathbf{L}_2$, and $\mathbf{L}_3$ defining the box as columns of an $\mathbf{L}$ matrix. Then

$$\dot{\mathbf{L}} = \boldsymbol{\kappa}^{\mathbf{T}}\mathbf{L}, \tag{11}$$

where $\boldsymbol{\kappa}^{\mathbf{T}}$ is the transpose of the velocity gradient tensor, given by

$$\boldsymbol{\kappa}^{\mathbf{T}} = \begin{pmatrix} \dot{\epsilon}_x & \dot{\gamma} & 0 \\ 0 & \dot{\epsilon}_y & 0 \\ 0 & 0 & \dot{\epsilon}_z \end{pmatrix}. \tag{12}$$

If at $t=0$, our unit cell is rectangular, i.e., $\mathbf{L}_1 \equiv (L_{1x},0,0)$, $\mathbf{L}_2 \equiv (0,L_{2y},0)$ and $\mathbf{L}_3 \equiv (0,0,L_{3z})$, then the solution of Eq. (11) is the following:

$$\mathbf{L}_1(t) = [L_{1x}(0)\exp(\dot{\epsilon}_x t),0,0], \tag{13a}$$

$$\mathbf{L}_2(t) = \left(\frac{\dot{\gamma}}{(\dot{\epsilon}_x - \dot{\epsilon}_y)} \{\exp[(\dot{\epsilon}_x - \dot{\epsilon}_y)t] - 1\} L_{2y}(0)\exp(\dot{\epsilon}_y t), L_{2y}(0)\exp(\dot{\epsilon}_y t), 0 \right)$$

$$\equiv \left(\frac{\dot{\gamma}}{(\dot{\epsilon}_x - \dot{\epsilon}_y)} \{\exp[(\dot{\epsilon}_x - \dot{\epsilon}_y)t] - 1\} L_{2y}(t), L_{2y}(0)\exp(\dot{\epsilon}_y t), 0 \right), \tag{13b}$$

$$\mathbf{L}_3(t) = [0,0,L_{3z}(0)\exp(\dot{\epsilon}_z(t)]. \tag{13c}$$

L_{1x}, L_{2y}, and L_{3z} are the box lengths in the three perpendicular directions changed by the elongation. There is, however, an additional nonzero term, L_{2x} which represents the deformation of the box under the impact of the shear. In practice, this term represents the displacement of the cells in the horizontal direction in the sliding brick implementation of this algorithm. This term, however, is different from one would intuitively assume by superposing the shear and elongational flow fields. Imagining the usual picture of sliding bricks one on the top of the other and assuming that the simultaneous presence of shear and elongational flow can be handled separately, this sliding term, L_{2x} would be

$$L_{2x}(t) = \dot{\gamma}\int_0^t L_{2y}(s)ds. \tag{14}$$

If one sets up simulations using Eq. (14) the resulting P_{xy} values will not reach a steady value but will tend to decay

exponentially. The stronger the shear field, the more pronounced this decay will be, as was found by Evans and Heyes.[3]

B. Possible improvements of elongational flow simulations

An advantage of the rotational equivalence described in the Introduction is that one can estimate PEF properties of systems from the much more economic PCF simulation by the SLLOD algorithm[8] as long as the $P_{yy}-P_{xx}\cong 0$ approximation is valid. Unfortunately, for more complex systems in the nonlinear regime this is not the case. The SLLOD algorithm for PCF simulations[8] is very elegant because it increments the streaming motion of particles at each timestep and handles explicitly only the random or peculiar velocities of particles. Supplemented with the Lees–Edwards boundary conditions[12] it is considered to be exact in the nonlinear regime too. It is then a matter of the thermostatting procedure chosen how far from the linear regime it is justified in its use. In the case of low Reynolds numbers, where the velocity profile is linear, even simple integral or differential feedback schemes, like Nosé–Hoover or Gaussian synthetic thermostats can be applied with confidence.[8]

The equations of motion for elongational flows can be written in a completely analogous fashion to PCF SLLOD equations,[3,4,5]

$$\dot{\mathbf{r}}_i=\frac{\mathbf{p}_i}{m}+\boldsymbol{\kappa}^T\cdot\mathbf{r}_i\,,$$
$$\dot{\mathbf{p}}_i=\mathbf{F}_i-\boldsymbol{\kappa}^T\cdot\mathbf{p}_i-\alpha\mathbf{p}_i\,, \tag{15}$$

where α is the thermostatting multiplier. Extensional flow simulations are started from equilibrium configurations by turning the field on instantaneously and then following the dynamics of the system for some time until steady state is achieved.[4,5] This should be repeated at least several hundred times from different equilibrium starting configurations in order to obtain reasonable statistics. The problem is the exponential decay and increase of box lengths discussed in the previous section. To obtain steady state values of system properties one should maintain constant elongational rate, i.e., exponential change in system dimensions for sufficiently long time to expect transients become negligible. During this time, however, the smallest system diameter should be larger than certain reasonable minimum. (At least the double of interaction cutoff distance between particles.) This requires large systems, in particular for high elongation rate simulations. A trivial way to reduce the demand for large systems is to change the simulation cell from the usual cube to a brick shape which has the smallest starting dimension in the direction of expansion and vice versa.[4] Here we propose a further possible improvement of this approach.

We are going to exploit that the simulated liquid is a nonlinear dynamical system which is very sensitive to small differences in initial conditions. Tiny displacements of particle positions generate exponentially separating trajectories. The distance of separation, d, of neighboring trajectories is characterized by the largest Lyapunov exponent, λ, as $d(t)\approx d(0)\exp(\lambda t)$ which is a physical property of the system.

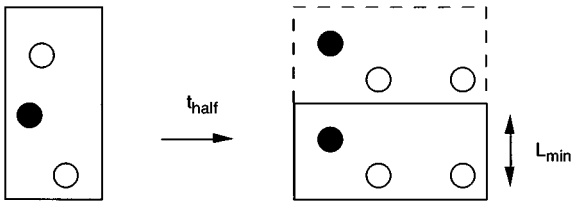

FIG. 2. A schematic picture of the doubling scheme.

The Lyapunov time, the time needed for two trajectories having almost identical starting positions in phase space, to become uncorrelated, however, depends also on the magnitude of the initial displacement and the accuracy of the calculations.[8]

Let our box lengths be $2L$ and L in the vertical and the horizontal directions, respectively (see Fig. 2). After a time, $t_{\text{half}}=\ln 2/\dot{\epsilon}$ the box lengths will be L and $2L$, respectively. If L is close to the smallest system dimension, $L_{\min}$, we can double our box length in the vertical direction by defining one set of images as real particles. When we are defining the images as real particles we add random displacements to their positions and velocities. These random displacements will ensure that after the Lyapunov time the upper half of the box will be uncorrelated with the lower half. Now, our system can evolve for another t_{half} time before approaching the size limit. Since the computation time is at least linearly proportional with the number of particles it is easy to show that repeating this procedure n times would provide a factor of $(2^{n+1}-1)/[(n+1)2^n]$ decrease in computer time compared to beginning the simulation with the same number of particles as at the end of n doubling procedures.

The doubling subroutine is compact and simple, and requires essentially no extra cost in computer time. The magnitude of random displacements should be a compromise between two opposite requirements; to be as large as possible to maximize $d(t)$ but small enough not to cause instability problems in the integrating routines and change the typical structure of the flowing system substantially. In our calculations we chose them in the order of 10^{-3} in reduced distances.

Unfortunately, if the elongation rate is very high there is no time for the image half of the box to evolve along a substantially different trajectory. After performing several exploratory runs, our conclusion is that the doubling scheme cannot be applied to elongation rates higher than ~ 0.5 in reduced rates.

A more easily solvable problem of shear free flow simulations by NEMD is related to the thermostatting mechanism of the system. The Nosé–Hoover thermostat provides results according to the canonical ensemble for equilibrium systems, so superficially it appears more attractive than the Gaussian thermostat which produces sharply defined kinetic energy with canonically distributed potential energy.[8] However, since it is an integral feedback, the Nosé–Hoover thermostat exhibits some delay in responding to suddenly changing conditions.

In Fig. 3 we show results of a PEF simulation, $\epsilon_x=0.3$,

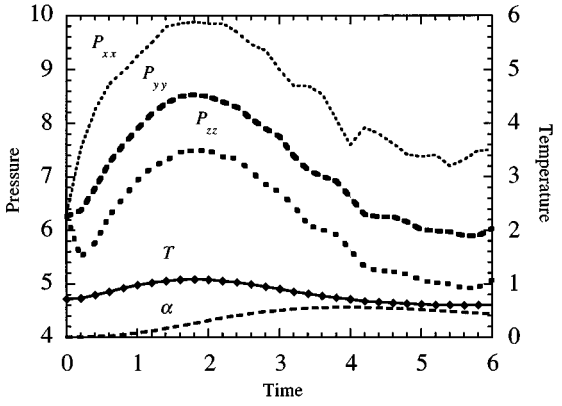

FIG. 3. Diagonal pressure tensor elements, temperature, and thermostatting multiplier as functions of time after an $\dot{\epsilon}_x=0.3$, $\dot{\epsilon}_z=-0.3$ elongation field was turned on at $t=0$. The curves are fitted to the points of every 50th timestep averaged over 375 independent trajectories. The delay in the response of the Nosé–Hoover thermostat is evident.

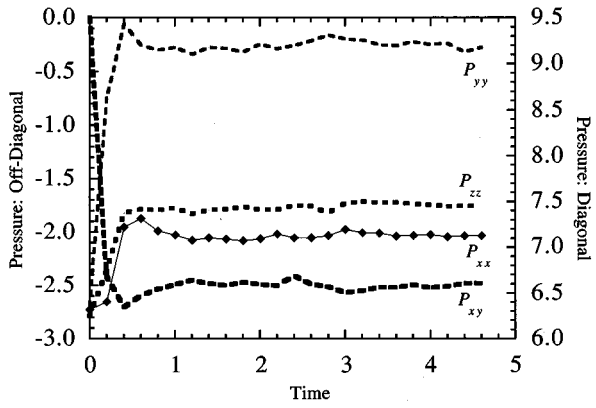

FIG. 5. The system is identical to that of Fig. 4. Nonzero elements of the pressure tensor are shown. All elements have a quickly approached steady state value.

$\epsilon_z=-0.3$, and $\epsilon_y=0.0$ using a Nosé–Hoover thermostat in both the equilibrium and nonequilibrium range. We are following the behavior of the system at equilibrium until time zero when we suddenly apply the velocity gradients. The external field heats up the system because the thermostat lags behind. This produces an unphysically large overshoot in terms of pressure and energy. Then the thermostatting multiplier catches up and starts to cool down the system. Since the plateau region is fairly short there is no time for the system to equilibrate. The actual energy and pressure values may be quite inaccurate. Obviously, their average value depends on from what time one starts to accumulate the average. The differences in pressure are less sensitive in this respect. This behavior was also noticed by Pierleoni and Ryckaert.[4]

We removed this problem by simply changing the thermostat in the elongational regime from Nosé–Hoover to Gaussian. This way we preserved the canonical equilibrium starting states but removed the uncertainty of averaging in the plateau region. In Fig. 4 we present the history of energy and temperature as the system changes from equilibrium to nonequilibrium steady state. The transition range is less than 1 time unit. In Fig. 5 we show the nonzero elements of the pressure tensor. In contrast to the findings of Ref. 3, we find that the response of the system to the combined shear and elongational field is steady with a well-defined plateau value.

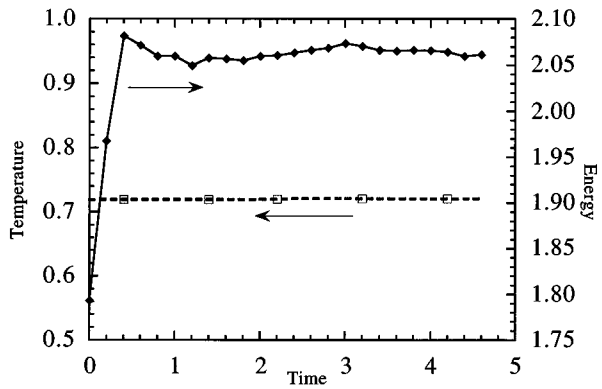

FIG. 4. Energy and temperature as function of time for a combined PCF and PEF simulation. $\dot{\gamma}=1.5$, $\dot{\epsilon}_x=0.3$, and $\dot{\epsilon}_y=-0.3$.

IV. DETAILS AND RESULTS OF CALCULATIONS

A. Shear and shear-free flows

Our calculations have been done at the same state point as for planar Couette flow. ($T=0.722$, $\rho=0.8442$). We began with an equilibrium system simulated with standard molecular dynamics. We used a Nosé–Hoover-type thermostat for this equilibrium system to have canonical starting states.[7,8] After every 40–80 timesteps we started a nonequilibrium trajectory with a constant elongation field turned on at $t=0$. These NEMD trajectories were calculated by the SLLOD equations with a Gaussian thermostat[14] maintaining the starting (equilibrium) temperature of the system. After a short time (<1.0) the transition reached a well-defined plateau region. Steady state averages were collected in this region for times, $t>1.0$. System sizes were in the range of $432\leqslant N\leqslant 1728$. Depending on N and the length of the plateau region which was $1.75\leqslant\Delta t_{\mathrm{pl}}\leqslant 5.0$, the number of NEMD trajectories were at least 350. For high strain rates we used only half of the usual timestep, $\Delta t=0.002$, in order to have higher accuracy.

In Fig. 6 we show the viscosities calculated for the four different, homogeneous flow fields in terms of the square-root of the strain rate. (Our plot is different from Fig. 1 of Ref. 4 because instead of the strain rate we have chosen the *square-root* of the strain rate as an independent variable and we have shown the BSF viscosities also on the positive half of the x-axis.) The shear viscosity values define an approximately linear line ending in the zero field limit value of 2.49. (Separate equilibrium Green–Kubo calculation gave 2.48 ± 0.02.) The PEF viscosities are always below this line and (with the exception of their last point at $\sqrt{\dot{\gamma}}=1.0$) these values give an excellent fit to another linear with a slope $\sqrt{2}$-times larger than that of the PCF viscosities.[4] In all four flows shear thinning is exhibited. At every strain rate and elongation rate studied for this system the sizes of the vis-

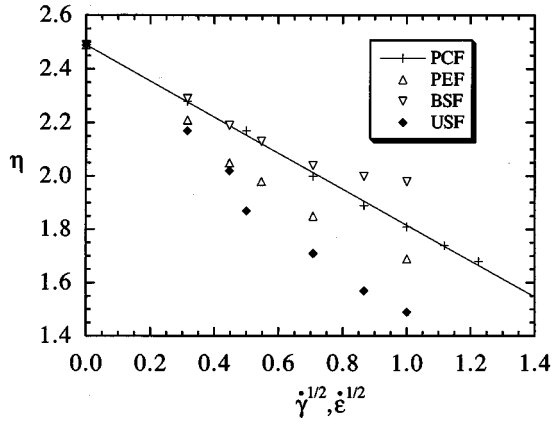

FIG. 6. Viscosities of different flows are shown as functions of the square-root of the strain rate. The linear is fitted to the shear flow viscosity values.

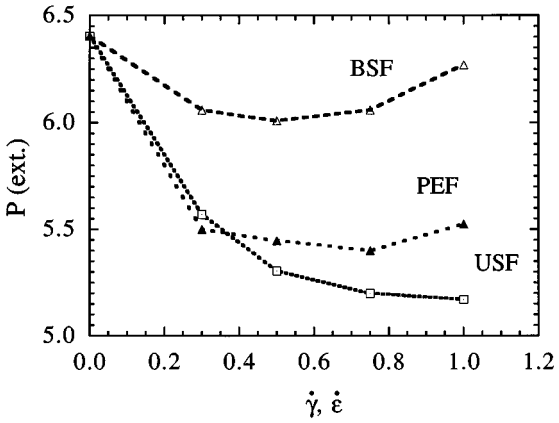

FIG. 8. The calculated pressure in the extension direction of the three extensional flows (PEF, USF, and BSF) in terms of the extension fields are shown.

cosity values follow the inequality $\eta_{\mathrm{USF}} \leqslant \eta_{\mathrm{PEF}} \leqslant \eta_{\mathrm{PCF}} \leqslant \eta_{\mathrm{BSF}}$. This is in accordance with what was found by Pierleoni and Ryckaert at a different state point of the same system.[4] At our state point, however, the BSF viscosities have no maximum in terms of the strain rate but decrease monotonically from the zero limit value. Nevertheless, in both simulations the behavior of BSF is the most different from PCF. While an approximate linear dependence of the viscosity on the square-root of the strain rate cannot be excluded in the case of USF either, this does not seem to be the case in BSF.

We also studied the energy and the pressure dependence of these flows in terms of the strength of the external field. (Since we used a differential feedback temperature control in the field-on part of our simulations we could measure these quantities without the uncertainties of oscillations in the plateau region.[4]) Uniform linear behavior of these quantities in terms of the second invariant of the strain rate tensor for all four flows is expected at small fields.[4] In Fig. 7 we present the internal energies. The internal energies of all these flows might comply with the approximate rule established for PCF claiming that the internal energy changes as $\gamma^{3/2}$. From the results shown in Fig. 6—with the exception of BSF—this seems reasonable. Very similar behavior was found for the average pressure of these flows. As in the case of the energy the following rule holds: $P_{\mathrm{PCF}} \leqslant P_{\mathrm{USF}} \leqslant P_{\mathrm{BSF}} \leqslant P_{\mathrm{PEF}}$. This is in accordance with the size of the second scalar invariant of the strain rate of the flows.[4] However, the USF values are always below the corresponding BSF values.

In the direction of extension the pressure has a minimum as a function of the strain rate as indicated in Fig. 8. The value of the strain field at which the extremum appears is the smallest for BSF. For USF, if the pressure in the extension direction does exhibit a minimum, it is beyond the extension rate of 1.0. In the direction of compression the flows show a monotonic increase in terms of the extension rate (see Fig. 9). Note that in Fig. 8 the USF pressure is close to the PEF pressure, while in Fig. 9 the BSF pressure is almost identical with the PEF pressure. This indicates a certain directional similarity between the shear-free flows in the case of simple fluids.

While the usual hydrostatic pressure, which is an average of the three coordinate directions, changed as $\gamma^{3/2}$ neither

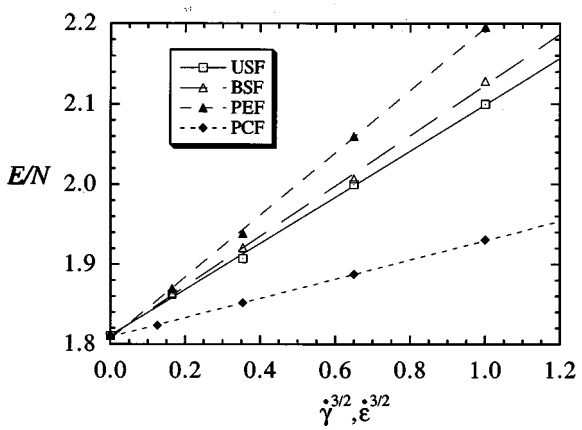

FIG. 7. Internal energies per particle in different flows are shown as functions of the 3/2 power of the strain field. The approximate linear fits match the calculated points reasonably well. The same behavior was found for the average pressure.

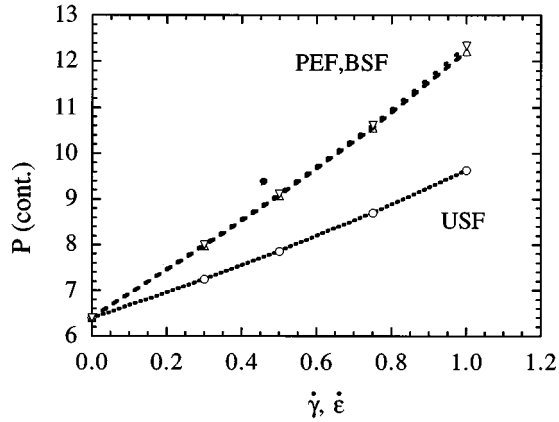

FIG. 9. The calculated pressure in the contraction direction of the three extensional flows (PEF, USF, and BSF) in terms of the extension fields are shown.

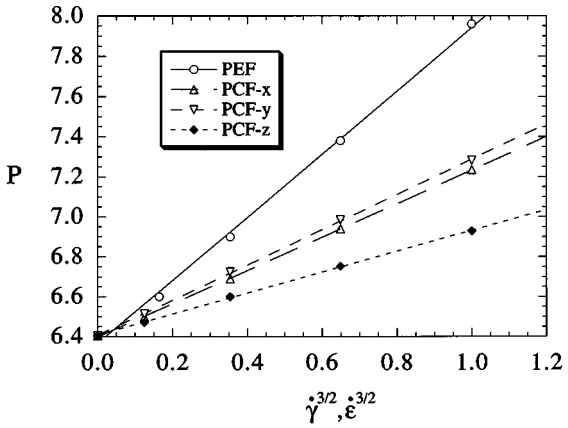

FIG. 10. Pressures in the three directions (x, y, and z, as defined in Fig. 1) for PCF. The pressure for PEF is shown for comparison.

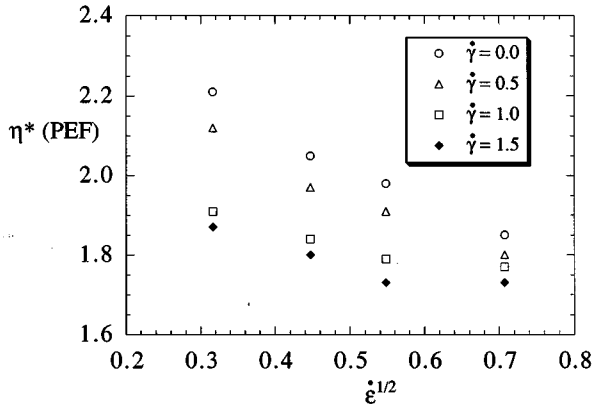

FIG. 11. PEF viscosities in the presence of shear field are shown in terms of the square root of the elongation rate.

the extension (Fig. 8) nor the compression (Fig. 9) direction alone exhibit this behavior. However, in the case of PCF this approximation is reasonable for the individual diagonal elements too (Fig. 10). In this graph we also show the direction of PEF which stays constant during the flow. This direction also seems to exhibit the approximate $\dot{\epsilon}^{3/2}$ behavior.

B. Combined shear and shear-free flows

Combined shear and extension fields are very common in polymer processing operations such as extrusion.[1] The present paper is motivated by the goal of developing simulation methodologies applicable to this combination of flow fields. In the case of combined flows we have adopted the usual frame convention for shear flow, streaming in the x direction with a velocity gradient in the y direction. The elongational directions are given with respect to this definition.

We report PEF computer simulations with $\dot{\epsilon}_x = \dot{\epsilon}$, $\dot{\epsilon}_y = -\dot{\epsilon}$, and $\dot{\epsilon}_z = 0.0$. In Table II we present the results of the calculations. We label the viscosities as if only one type of field was acting, so that

$$\eta(\mathrm{PEF}) = (P_{yy} - P_{xx})/4\dot{\epsilon}, \tag{16a}$$

$$\eta(\mathrm{PCF}) = -P_{xy}/\dot{\gamma}. \tag{16b}$$

The viscosity defined in Eq. (7) is given in terms of these quantities by

$$\eta = [8\dot{\epsilon}^2 \eta(\mathrm{PEF}) + 2\gamma\eta(\mathrm{PCF})]/(8\dot{\epsilon}^2 + 2\gamma). \tag{17}$$

The shear and the elongation takes place in the same plane (see Fig. 1). According to the arguments of the previous sections it is not surprising that the superposition of the two flow fields in this arrangement produces more pronounced shear thinning for both flows. In Fig. 11 we show the η(PEF) values in terms of the square root of the elongation rate. The simultaneous presence of the shear field reduces the elongational viscosities, with stronger shear resulting in more substantial reduction.

Finally, we show results for combined BSF and PCF flows (Fig. 12). The system extended into the x and z and contracted in the y-directions. Here we show the BSF vis-

TABLE II. Results of PEF and combined PEF and PCF flows. The errors estimated in the viscosities are ±0.04.

PEF field ($\dot{\epsilon}$)	PCF field ($\dot{\gamma}$)	η (PEF)	η (PCF)
0.1	0.0	2.21	⋯
0.2	0.0	2.05	⋯
0.3	0.0	1.98	⋯
0.5	0.0	1.85	⋯
0.1	0.5	2.12	1.96
0.2	0.5	1.97	1.95
0.3	0.5	1.91	1.87
0.5	0.5	1.80	1.75
0.1	1.0	1.91	1.79
0.2	1.0	1.84	1.80
0.3	1.0	1.79	1.76
0.5	1.0	1.77	1.70
0.1	1.5	1.87	1.68
0.2	1.5	1.80	1.68
0.3	1.5	1.73	1.67
0.5	1.5	1.73	1.63

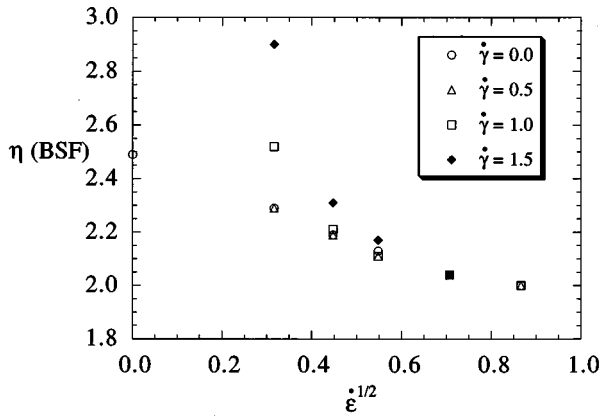

FIG. 12. Elongation viscosities calculated from the diagonal elements of the pressure tensor in BSF in the presence of shear in terms of the square root of the elongation rate.

cosities in the presence of PCF fields of different strengths. (The PCF viscosities are less sensitive in the case of a simultaneous BSF field.) At low BSF fields the high shear rate enhances the extension viscosities considerably. This effect comes from the fact that high shear fields produce differences in diagonal pressure tensor elements. These so-called normal stress differences then change the *apparent* viscosity of the superimposed shear free flow because the latter is calculated from the diagonal elements of the pressure tensor. This effect is the largest for high shear and small extensional fields.

V. CONCLUSIONS

We have examined and compared the properties of shear and shear-free flows in simple liquids. We proposed that for simple fluids the two planar flows (PCF and PEF) are rotationally equivalent even in the nonlinear regime. The basic rationale for this proposed rotational correspondence of PEF and PCF flows for atomistic (spherically symmetric) fluids can be understood if one takes into account that the flow field of PCF can be viewed as a sum of a rotational and an elongational field. Since the particles are spherically symmetric the rotational part plays only very small role in the flow. (This is definitely not the case for molecular fluids, and especially not the case for polymer melts.)

It is worthwhile to analyze our results from the phenomenological point of view. In NEMD simulations it is usual to study and interpret rheological data using the familiar Newtonian constitutive relation of Eq. (7). Then high flow field results are presented and discussed with respect to the zero field limit behavior. In theoretical descriptions of the complex rheological properties of polymeric fluids, it is customary to use more complex nonlinear and/or memory-dependent phenomenological models. In the following we invoke such a model described by Astarita and Marucci[13] to show that although simple fluids show non-Newtonian behavior for sufficiently high shear rates, their properties still can be described by a fairly simple model.

The most general nonlinear but still memory independent (i.e., instantaneous) and local constitutive relation can be written as

$$\boldsymbol{\sigma}=\mathbf{g}(\dot{\boldsymbol{\gamma}}). \tag{18}$$

A theorem from tensor analysis states that any isotropic symmetric tensor function $\mathbf{g}$ can only be of the form

$$\mathbf{g}(\dot{\boldsymbol{\gamma}})=\phi_0\mathbf{1}+\phi_1\dot{\boldsymbol{\gamma}}+\phi_2\dot{\boldsymbol{\gamma}}^2, \tag{19}$$

where the ϕ-*s* are scalar functions of the three principal invariants of $\dot{\boldsymbol{\gamma}}$. Taking into account that we are dealing with constant density fluids, Eq. (19) simplifies to the following:

$$\boldsymbol{\sigma}=\phi_1(\mathrm{II},\mathrm{III})\,\dot{\boldsymbol{\gamma}}+\phi_2(\mathrm{II},\mathrm{III})\,\dot{\boldsymbol{\gamma}}^2, \tag{20}$$

where II and III are the second and third invariants of the strain-rate tensor. From this equation for the components of the stress tensor the following relations are obtained:

$$\begin{aligned}&\sigma_{12}=\sigma_{21}=\phi_1\dot{\gamma},\\ &\sigma_{13}=\sigma_{31}=\sigma_{23}=\sigma_{32}=0,\\ &\sigma_{11}-\sigma_{22}=0,\\ &\sigma_{22}-\sigma_{33}=\phi_2\dot{\gamma}^2.\end{aligned} \tag{21}$$

For our WCA fluid at this state point

$$\phi_1=\eta_0-\eta_1\dot{\gamma}^{1/2}\ \text{ and }\ \phi_2=\eta_{23}\dot{\gamma}^{-1/2}, \tag{22}$$

where $\eta_0=2.49$, $\eta_1=0.67$, and $\eta_{23}=0.34$. Fluids obeying relationships (19)–(21) are known as Reiner–Rivlin fluids.[13] The description of their flow behavior does not require invoking memory-dependent relationships between the stress and the strain. Within a very good approximation, the WCA fluid of spherically symmetric particles is a Reiner–Rivlin fluid. Indeed, the characteristic relaxation time for these fluids is only a couple of hundred timesteps which in real time (for liquid argon, for example) corresponds to $\approx 10^{-12}$ s.

It is also instructive to consider the implications of this approximation from a microscopic point of view. In the kinetic theory of dilute polymer solutions it is customary to model the rotation free deformation (the elongation) of a molecule by steady state potential flow fields.[1] In these calculations the configurational distribution in the flow is found explicitly by assuming that the phase space distribution function can be written as the product of the configuration space distribution function and the velocity space distribution function. It is then assumed further that the velocity space distribution is Maxwellian at the center of mass of the molecule, and the configuration space distribution function is independent of the location of the center of mass of the polymer molecule. The most general solution of this problem for steady state, homogeneous, potential flow of a dilute solution of dumbbells with any physically reasonable spring force law is[1]

$$\Psi(\mathbf{Q})=\left[\frac{1}{J_{\mathrm{eq}}}e^{-\Phi(c)/kT}\right]\left[\frac{J_{\mathrm{eq}}}{J}e^{(\zeta/4kT)(\boldsymbol{\kappa}:QQ)}\right], \tag{23}$$

where the first term is the equilibrium distribution function, J_{eq} and J are normalization constants for the equilibrium and nonequilibrium distribution functions, respectively; ζ is an isotropic friction coefficient, $\boldsymbol{\kappa}$ is a tensor describing the flow field, and $\mathbf{Q}$ is the dumbbell connector vector.

The terms in the exponential of Eq. (23) is reminiscent of the Hamiltonian of the DOLLS equations of homogeneous shear flow,[14]

$$H=H_0+\sum_{i=1}^{N}\mathbf{q}_i\mathbf{p}_i:\boldsymbol{\kappa}^T. \tag{24}$$

Historically, the equations of motion derivable from the DOLLS Hamiltonian have been superseded by the closely related SLLOD equations. The latter are not derivable from a Hamiltonian but are considered to be an exact representation of homogeneous shear flow.[8] Both the DOLLS and SLLOD equations of motion have the same dissipation and give the correct linear behavior, but the DOLLS tensor algorithm begins to yield incorrect results at quadratic order in the strain rate. These errors first show up in the normal stress differences. For irrotational flows the two methods are identical.[8] Since for spherically symmetric particles the rotational part

of the flow field produces only very small effects, the flow can be approximated as a pure potential flow even outside the linear regime.

In the following we are going to show that the DOLLS tensor Hamiltonian can be simplified into the form of a potential flow. Let us consider explicitly only two particles in the system. These particles have identical masses and can be considered to be the two beads of the dumbbell molecule. Let us fix the center of mass to be at the original and the total momentum of this system to zero, i.e., $\mathbf{p}_1=-\mathbf{p}_2=\mathbf{p}$ and $\mathbf{q}_1=-\mathbf{q}_2=\mathbf{q}$. Then

$$H=H_0+2\boldsymbol{\kappa}:\mathbf{qp}=H_0+\boldsymbol{\kappa}:\mathbf{Qp}, \tag{25}$$

where we have exploited the definition of the dumbbell bond vector $\mathbf{Q}\equiv\mathbf{q}_1-\mathbf{q}_2=2\mathbf{q}$. Taking into account the approximations used in Eq. (23) we can remove the momentum from Eq. (25). (Note that the factorization of the distribution function into velocity and configuration dependent parts is a poor approximation for systems in the nonlinear regime. Even the assumption of a Maxwellian distribution of peculiar velocities around the local streaming velocity is not valid.[15] If we take into account, however, that the reduced strain rates are at least an order of magnitude larger than the highest attainable strain rates in realistic experiments[16] because the natural limit for the speed of heat removal is not experienced in simulations using infinitely fast synthetic thermostats, then the approximation is not as poor as it seems at first glance.) In the Langevin picture the average of the momentum at time t is given

$$\langle\mathbf{p}(t)\rangle=\exp(-t\zeta'/m)\mathbf{p}(0) \tag{26}$$

if one assumes the starting value of $\mathbf{p}(0)$. Integrating Eq. (26) by time

$$\langle\mathbf{q}(t)\rangle-\mathbf{q}(0)=\int_0^t ds\ \exp(-s\zeta'/m)\mathbf{p}(0)$$

$$=-\frac{m}{\zeta'}[\langle\mathbf{p}(t)\rangle-\mathbf{p}(0)]. \tag{27}$$

Clearly, Eq. (27) is valid for any t and $\mathbf{p}(0)$ value. Now, taking into account that when Eq. (23) was derived no explicit masses were used (i.e., ζ and ζ' are related by $\zeta=\zeta' m$), the combination of Eqs. (25) and (27) yields essentially a Hamiltonian of the form $H=H_0-(1/2)\zeta\boldsymbol{\kappa}:\mathbf{QQ}$ which leads to the exponent of Eq. (23). (The additional factor of 1/2 comes from a slightly different definition of the flow field.[1])

We have shown that the properties of simple liquids in PEF are closely related to those in PCF. Although there is no such close relationship between all four type of flows, their behavior in terms of strain rate dependence is still very similar. As a first approximation their viscosities can be given as linear functions in terms of $\dot{\gamma}^{1/2}$ and their internal energies and average pressures as linear functions of $\dot{\gamma}^{3/2}$.

We identified two interesting features of shear-free flows. The first is the extremum behavior of the pressure in the expansion direction of the flow. The second is the directional similarity of elongation flows. The extending direction of PEF behaves like the extending direction of USF, while the contracting direction of PEF produces almost identical effects as the contracting direction of BSF. This directional similarity is more clear from studies of the microscopic dynamics of the flows[17] manifested in the velocity autocorrelation function of particles, but the similar numerical values of the corresponding pressure elements already indicate this property. In the case of PEF one direction expands with ϵ, another direction shrinks with $-\epsilon$ while the third direction stays constant. In USF one direction expands with ϵ while the two other direction contracts with $-\epsilon/2$. The similarity of microscopic dynamics in the expansion direction of these two flows means that the impact of the two other directions is quite indirect, averaged out. The same can be said about the microscopic dynamics of the PEF and BSF contraction directions.

We also performed combined PCF and PEF simulations when the stretching of the simulation cell was in the flow direction and the direction of the (constant) streaming velocity gradient and the compression were identical. Not surprisingly, the simultaneous presence of these two coplanar fields produced further shear thinning, particularly in the elongational viscosity. In the case of the combined PCF and BSF flow in the studied geometry the coupling of the two fields was less pronounced.

The introduction of these different flow patterns was done with the purpose to describe the complex behavior of polymeric liquids.[1] Although at very high shear rates simple liquids are markedly non-Newtonian, their behavior is still reasonably simple. This study can serve as a reference to further investigations when molecular and polymer systems are modeled at microscopic level.

ACKNOWLEDGMENTS

A.B. thanks the financial support of OTKA Grant No. F7218. P.T.C. gratefully acknowledges support of this research by the National Science Foundation through Grant No. CTS-9101326 and by Martin Marrietta Energy Systems at Oak Ridge National Laboratory through the Distinguished Scientist program.

[1] R. B. Bird, C. F. Curtiss, R. C. Armstrong, and O. Hassager, *Dynamics of Polymeric Liquids*, 2nd ed. (Wiley, New York, 1987), Vols. I and II.
[2] D. M. Heyes, Chem. Phys. **98**, 15 (1985); Phys. Lett. **115**, 42 (1986).
[3] M. W. Evans and D. M. Heyes, Mol. Phys. **69**, 241 (1990).
[4] C. Pierleoni and J. P. Ryckaert, Phys. Rev. A **44**, 5314 (1991).
[5] M. N. Hounkonnou, C. Pierleoni, and J. P. Ryckaert, J. Chem. Phys. **97**, 9335 (1992).
[6] J. P. Hansen and I. R. McDonald, *Theory of Simple Liquids*, 2nd ed. (Academic, New York, 1987).
[7] M. P. Allen and D. J. Tildesley, *Computer Simulation of Liquids* (Clarendon, Oxford, 1987).
[8] D. J. Evans and G. P. Morriss, *Statistical Mechanics of Nonequilibrium Liquids* (Academic, New York, 1990).
[9] B. L. Holian and D. J. Evans, J. Chem. Phys. **78**, 5147 (1983).
[10] M. Born, Z. Phys. **1**, 221 (1920).
[11] R. Edberg, D. J. Evans, and G. P. Morriss, Mol. Phys. **62**, 1357 (1987).
[12] A. W. Lees and S. F. Edwards, J. Phys. C **5**, 1921 (1972).
[13] G. Astarita and G. Marucci, *Principles of Non-Newtonian Fluid Mechanics* (McGraw-Hill, New York, 1974).
[14] W. G. Hoover, D. J. Evans, R. B. Hickman, A. J. C. Ladd, W. T. Ashurst, and B. Moran, Phys. Rev. A **22**, 1690 (1980).
[15] W. Loose and S. Hess, Physica **174**, 47 (1991).
[16] S. Y. Liem, D. Brown, and J. H. R. Clarke, Phys. Rev. A **45**, 3706 (1992).
[17] A. Baranyai and P. T. Cummings, Mol. Phys. (in press).